Informatics in Medicine Unlocked 58 (2025) 101682

Contents lists available at ScienceDirect

Informatics in Medicine Unlocked

journal homepage: www.elsevier.com/locate/imu

Hybrid quantum neural networks for computer-aided sex diagnosis in forensic and physical anthropology

Asel Sagingalieva [a], Luca Lusnig [a,b], Fabio Cavalli [b], Alexey Melnikov [a,*]

[a] Terra Quantum AG, 9000 St. Gallen, Switzerland
[b] Research Unit of Paleoradiology and Allied Sciences, Laboratorio di Telematica Sanitaria-Struttura Complessa Informatica e Telecomunicazioni, Azienda Sanitaria Universitaria Giuliana Isontina, 34149 Trieste, Italy

ARTICLE INFO

Keywords:
Hybrid quantum–classical neural networks
Forensic anthropology
Sex Determination
Machine learning in anthropology
Variational quantum circuits
Quantum Processing Unit

ABSTRACT

The determination of sex from skeletal remains is essential for forensic science and the reconstruction of demographic patterns in ancient communities. This study aims to develop and evaluate hybrid deep-quantum neural network architectures to improve the accuracy and robustness of sex estimation from calvarium shape data. Deep learning has reached new heights in a number of scientific fields, while quantum techniques have the potential to process data in unique ways, offering benefits such as parallel processing and superposition. In the study, we investigate how an integration of deep learning and quantum computing will optimize sex estimation based on the shape complexity of calvarium, specifically through the algorithm based on Fast Fourier Transform of calvarium shapes. In previous studies with the same data, the highest achieved accuracy was 82.25%, utilizing classical machine learning and neural networks, such as Multilayer Perceptron. To improve the performance, we used four different neural network models: the classical Multilayer Perceptron and Convolutional Neural Network, along with Hybrid Quantum Classical Neural Networks, including Hybrid Quantum Classical Convolutional Networks on the morphological variations of the curve representing the sagittal profile of the calvarium. All the models outperformed the experts and improved the previous findings, achieving over 82.4% accuracy. Furthermore, the experiments on stability and accuracy over small datasets showed that one of proposed hybrid networks outperforms classical analogue on a small amount of data. The final performance of the hybrid models is better than the classical results and the best result achieved is 87.4%. We also launched the best hybrid model on the QPU, and the achieved accuracy of 90.71% is comparable to the classical simulation at 92.14%. Our research benefited significantly from new tools for analyzing quantum variational algorithms, which are inaccessible to classical methods, enabling us to reach higher results. This study not only demonstrates success in solving the specific task but also opens new possibilities for the application of quantum technologies in anthropology.

1. Introduction

A fundamental task of physical and forensic anthropologists is to reconstruct the biological identity of human remains from the often incomplete information provided by the skeleton or parts of it [1]. Methods for sex determination from bone remains are numerous and based on visual inspection of morphological characters or through quantitative methods generally based on linear measurements. The bones traditionally considered most dimorphic are primarily the pelvis and skull, although very good results can be obtained with other elements of the postcranial skeleton [2].

The study of the sexual dimorphism of the skull is constantly being investigated for anthropological and forensic purposes and is generally based on direct measurement of the skull [3,4], teleradiographic projection [5], volumetric cranial CT [6] or three-dimensional digitization of the skull [3,7]. It is worth emphasizing that cephalometric variables must be extracted manually by direct measurement by an experienced anthropologist, and no reliable system for automatic extraction of such measurements has been implemented at present. It follows that a potentially operator-independent expert system should be based on direct reconnaissance of the cranial shape.

* Corresponding author.
E-mail address: alexey@melnikov.info (A. Melnikov).

https://doi.org/10.1016/j.imu.2025.101682
Received 16 March 2025; Received in revised form 26 July 2025; Accepted 10 August 2025
Available online 26 August 2025

Such approaches have been already incorporated in anthropology [8], demonstrated their effectiveness in traditional craniometry systems [9] and shape analyses of the cranial vault [10,11].

The work presented in [10] demonstrates the application of classical machine learning approaches to forensic anthropology tasks, specifically the complex challenge of sex determination based on the lateral shape of the calvarium. The authors employed several classical methods to the dataset consisting of Fourier descriptors of initial MDCT scanograms and achieved a commendable accuracy of 82.25% with cross-validation using their best model — Multilayer Perceptron (MLP). In contrast, our study introduces new approaches that surpass the previously reported accuracy, with the best model achieving a high score of 87.7% under the same conditions. Additionally, we evaluate the models on a reduced dataset, which is particularly relevant in scenarios with limited data availability — cases that often occur in forensic anthropology. This advancement opens up new avenues for future research in the field.

Our paper introduces Quantum Machine Learning (QML) to the task of forensic anthropology, an approach that combines quantum computing ideas with machine learning techniques [12–14]. In particular, QML brings novelty by joining operations on quantum instances, such as Quantum Bits (qubits), and classical deep learning architectures, introducing Hybrid Quantum Classical Neural Networks (HQNNs). This integration has the potential to boost computational effectiveness and algorithm's accuracy.

In our study, we tackle the challenge of sex diagnosis from the lateral shape of the calvarium using a dataset consisting of scanograms. We employed two HQNNs: Parallel Hybrid Network (PHN) and a Hybrid Quantum Convolutional Network (HQCNN). The main quantum component of our purposed HQCNN is Quanvolutional Neural Network Layer (QuanvLayer). We compared the HQNNs with their classical counterparts MLP and Convolutional Neural Network (CNN). All the methods demonstrated accuracy exceeding 80%, which is comparable or even exceeds the performance of experienced anthropologists. Notably, both PHN and HQCNN outperformed classical models in terms of accuracy and precision–recall metrics. Furthermore, PHN demonstrated greater stability and accuracy across reduced datasets. What is more remarkable is that the best-trained PHN was executed on a quantum processing unit (QPU) [15], achieving a result of 90.71%, which is closely comparable to the 92.14% obtained from the classical simulation. These outcomes highlight the effectiveness of the HQNN in anthropological analyses.

This study focuses on a practical application in forensic and physical anthropology: sex determination based on the shape of the cranial vault. By improving the accuracy of automatic classification using HQNNs, our approach may assist forensic experts in the analysis of unidentified human remains. In particular, the system is designed to be integrated into computer-aided diagnosis tools for use in archaeological contexts or forensic investigations, where skeletal remains are incomplete or degraded. The broader aim is to develop quantum-enhanced methods that can augment expert judgment in anthropology while operating effectively under real-world constraints.

Our hybrid models have potential applications beyond their immediate use. We see HQNN as a valuable tool for anthropologists, providing enhanced accuracy and efficiency in sex determination tasks and helping to advance research methods in anthropology. Moreover, our work represents an important step forward in the development of QML applications, paving the way for collaboration and innovation across different fields within anthropology and forensic science.

The remainder of this paper is organized as follows. Section 2 ("Materials and Methods") presents the dataset, preprocessing steps, and the design of both hybrid quantum and classical neural network architectures. Section 3 ("Training and Results") details the training procedures and reports the performance metrics of all models, including experiments with quantum hardware. Section 4 ("Discussion") reflects on the implications of the results, situates them within the broader context of forensic anthropology and quantum machine learning, and includes a subsection on limitations and future challenges. Finally, Section 5 ("Conclusion") summarizes the key findings and contributions of the study.

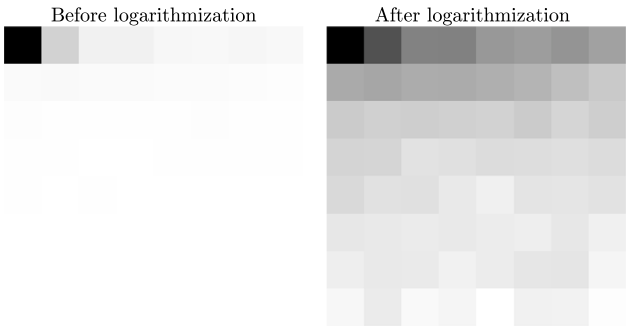

Fig. 1. A sample of a preprocessed male skull image. (Left) Fourier descriptor representation of the original skull contour. (Right) Log-transformed version of the same descriptor used as input to the models.

2. Materials and methods

2.1. Dataset of skulls

The dataset used is the same as that used in the study by Ref. [10]. This dataset consists of 1400 lateral scout-view MDCT scanogram equally divided between male and female adult subjects, and given the premises anthropological, of a population of individuals that is as homogeneous possible. The lateral MDCT scanograms were transformed from DICOM to JPG format, maintaining the original matrix size, that is 512×512 gray-scale pixels with 8-bit resolution. An example of this image is shown in Fig. 2(a).

Preprocessing for feature extraction was applied to each image, where first a Gaussian smooth filter [16] and a sharpening filter [17] were applied to eliminate additive noise and highlight the contrast of the bone profile, and then a Canny algorithm [18] determined the profile of the cranium (Fig. 2(a)). The obtained contour of about 450 pixels was sampled by obtaining 128 equidistant points [19] whose distance from the centroid [20] was calculated to obtain the Fourier descriptors [20] used as representative values of the image.

The final dataset sample is depicted in Fig. 1. One can see that the sample's features appears denormalized and it can affect the performance of the future models. Thus, the last data preprocessing step involved logarithmization – taking logarithms of the tenzors to make features distincter.

2.2. Hybrid quantum neural networks for image processing

Machine learning algorithms find huge development and application fields recent years, becoming a key tool for data analysis [21], text generation [22], and other tasks. Taking roots from statistics, probability theory and linear algebra, machine learning is incredible at handling complex tasks, especially in classification, making it a popular choice in anthropological studies and forensic science [23,24], specifically in sex determination tasks [25–28].

QML represents an innovative intersection of quantum mechanics and machine learning techniques [29]. Its key advantages over classical methods arise from the unique properties of quantum phenomena, particularly entanglement and superposition [30,31]. Entanglement enhances the interconnectedness of quantum components, allowing for simultaneous exploration and evaluation of various possibilities, which can lead to more efficient problem-solving. Superposition enables QML systems to operate in multiple states at once, significantly increasing

computational parallelism and improving the effectiveness of information analysis. This combination establishes QML as a powerful approach for addressing complex problems in artificial intelligence.

The field of QML is actively developing presenting several QML architectures that provide complementary routes to expressive yet trainable models. Quantum support vector machines leverage quantum linear-algebra subroutines to perform classification with potential exponential speedups in feature dimension [32]. Quantum kernel methods leverage quantum circuits to map classical data into high-dimensional Hilbert spaces, enabling classical algorithms to perform convex optimization tasks such as classification and regression [33]. This hybrid approach has demonstrated competitive performance across various benchmarks, as detailed in recent studies [34–36]. Quantum convolutional neural networks (QCNNs) have been developed as fully quantum analogs of classical CNNs, employing quantum circuits to perform convolution and pooling operations for image classification tasks, demonstrating improved performance compared to traditional approaches [37–39].

Despite the promise of QML, quantum neural networks encounter both theoretical and hardware limitations. One of the main obstacles these networks face today is the noise-free barren plateau problem [40]. Hardware issues, including the limited number of qubits, accuracy constraints [15,41], and susceptibility to noise and external disturbances pose substantial hurdles [42]. To address these challenges, recent studies have proposed several mitigation strategies, including layer-wise training methods [43], locality-aware cost functions [44], entanglement-restricted ansätze [45], identity-initialized blocks [46], and noise-aware regularization techniques [47]. These approaches collectively help to maintain meaningful gradient magnitudes and improve convergence rates on real quantum hardware.

HQNNs combine classical and quantum components to balance efficiency and expressivity, presenting a promising solution to the challenges posed by quantum approaches. HQNNs leverage the strengths of both classical and quantum neural networks, offering faster convergence and improved accuracy compared to their classical counterparts [48–52]. Notably, HQNNs have gained attention in various industries and scientific applications, including finance [53], photovoltaics [54], fluid dynamics [55], drug response prediction [48], routing problems [56] and other domains [57,58]. A recent study [59] presented a hybrid quantum image classification architecture combined with federated learning for diagnosing hepatic steatosis, achieving 97% accuracy with significantly fewer parameters than classical baselines. Another work proposed a hybrid framework that integrates classical convolutional neural networks with quantum classifiers to detect respiratory diseases from chest X-ray images, showing high accuracy on large-scale real-world datasets and successful deployment on quantum hardware [60]. The synergy achieved by combining classical and quantum elements in HQNNs makes them a compelling approach for addressing the intricacies of anthropological research tasks.

Recent research has also applied HQNNs to biomedical and healthcare tasks, highlighting their relevance for sensitive and data-limited domains. One study [61] introduced a hybrid quantum–classical optimization framework aimed at building energy-efficient edge architectures in RIS-assisted AIoT healthcare, achieving improved classification performance under real-world constraints. Another work [62] proposed a quantum-inspired heuristic method for secure healthcare prediction using blockchain technology, with results demonstrating improved robustness on small and noisy datasets. In the context of medical imaging, a quantum-enhanced convolutional model was developed for breast cancer diagnosis [63], outperforming classical CNNs in classification accuracy. Additional work [64] focused on hybrid quantum–classical graph neural network for tumor classification in digital pathology, demonstrating comparable performance to state-of-the-art classical models while efficiently handling high-dimensional features using a logarithmic number of qubits. Together, these advances confirm HQNNs' growing potential for complex diagnostic and classification problems in biomedical domains, supporting their use in forensic anthropology.

The advancements in HQNNs provide several benefits over traditional neural networks. The proposed PHN architecture allows for the simultaneous use of MLP and the Quantum Depth Infused (QDI) layer, which will be introduced later, enhancing the model's expressiveness and effectiveness. The QDI layer excels at processing high-dimensional input vectors effectively addressing current technological constraints. Furthermore, HQCNNs, when combined with Fourier transforms (FT), demonstrate superior performance compared to classical CNNs. These innovations open new avenues for applications in physical and forensic anthropology, potentially improving methodologies and technologies in the field.

2.2.1. Parallel hybrid network

Efficiently harnessing both the complementary strengths of classical and quantum components, we employ a Parallel Hybrid Network (PHN) [65]. Hybrid architectures can integrate quantum layers either sequentially or in parallel; by adopting the parallel design, our PHN avoids the gradient-vanishing and information-bottleneck issues often seen in sequential hybrids [65]. Furthermore, PHN has already shown excellent performance across diverse tasks, including steam mass flow forecasting [66], image classification [67], and drug response prediction [48]. This established versatility and effectiveness motivated our selection of this particular hybrid architecture.

In a PHN, the same input vector is processed simultaneously by MLP and a Variational Quantum Circuit (VQC). MLPs are known for producing non-harmonic functions, while VQCs fit smooth truncated Fourier series. By combining these outputs, PHNs leverage the strengths of both methods, capturing intricate patterns and relationships within data for enhanced performance compared to using a single MLP. Taking into consideration the fact, that the dataset used in our study consists of Fast Fourier Transforms of the calvarium shape, the PHN's ability to integrate periodic and nonlinear patterns makes it especially well suited to this task.

The architecture of our PHN, depicted in Fig. 2(b), seamlessly integrates two parallel models: MLP and a quantum layer, where the quantum layer is a specially designed VQC known as the QDI layer [48]. This quantum component is designed to address the challenge of processing large datasets with a limited number of qubits. Instead of encoding each feature on a separate qubit, QDI employs a data re-uploading method to form a lattice of features and encode them sequentially. Variational quantum layers and entangling gates between different encoding parts allows the model to learn complex patterns and correlations, enhancing its expressiveness. By combining the QDI's efficient, sequential encoding of high-dimensional features with parallel classical processing and a final integration of a classical layer, the PHN produces richer joint representations from quantum and classical outputs and, in theory, offers greater expressivity than a traditional fully connected network.

2.2.2. Hybrid quantum convolutional network

Another model developed in the study is HQCNN which incorporates a special type of transformation layers – QuanvLayer [68]. HQCNN is inspired by CNN, while using QuanvLayer instead of a convolutional one. Prior works show that a single QuanvLayer can achieve great results in various classification tasks [69–71]. For instance, recent research [67] has demonstrated that the use of QuanvLayer, in comparison to a single CNN layer, yields better results in terms of accuracy. Another study [72] indicates that using hybrid quantum–classical model, namely Quantum Fourier Convolutional Network helps to achieve exponential speed-up, while being compared with CNN. These findings make HQCNN an attractive choice for our Fourier-based skull-contour data.

Unlike traditional CNNs, HQCNNs extract local features through quanvolutional filters implemented as shallow, few-qubit VQCs that together present a QuanvLayer. This layer encodes spatially local patches

of input into a small register of qubits, applies parameterized rotations and entangling gates, and then measures the qubits to produce a transformed feature map. This approach is particularly advantageous given current hardware limits — QuanvLayer filters require a small number of qubits and minimal circuit depth, while yielding rich frequency-domain representations. By combining these quantum-derived maps with classical convolutions, HQCNN can capture intricate data patterns, potentially revealing features that pure CNNs might miss.

Considering all the benefits of utilizing quanvolutional layers along with convolutional ones, including proven empirical performance, compatability with current hardware, potentially enhanced expressivity, we develop a hybrid model which is highly effective for the sex determination task, achieving results superior to traditional CNNs. The architecture of our HQCNN, as shown in Fig. 2(c), incorporates a sequence of MLP, QuanvLayer, and classical convolutional layers, concluding with a linear output layer for male/female classification. This structure, as proven by results, enables efficient feature extraction and pattern differentiation between male and female samples.

2.3. Neural networks for image processing

The deep learning algorithm incorporated in our research for comparison with the presented hybrid quantum–classical approach PHN is MLP. The architecture of MLP contains multiple layers of nodes, each connected to every node in the next layer. MLP was first proposed as an algorithm for solving linearly non-separable problems and developed the idea of the single-layer perceptron, which is equivalent to linear regression. Later, the idea of MLP was developed and popularized, through the introduction of the backpropagation [73].

Research in craniometry [9] and cranial vault shape analysis [10, 11] has revealed that MLPs effectively capture several patterns, making them suitable for our sex classification task. We chose the MLP as our primary classical baseline because its stack of fully connected layers with nonlinear activations most closely matches the structure of our PHN (which alternates between quantum and classical layers), allowing us to quantify the benefit of the quantum component.

Another technique used in the study for comparison with HQCNN is CNN. Well-known and widely used for image recognition, along with other tasks involving data with geometrical patterns and visual structures (e.g., grid-like data), CNN has proven effective in similar applications [74]. We included CNN as the classical counterpart to HQCNN. Its local filters and hierarchical feature extraction are similar to the quanvolutional layers, allowing a clear comparison of how quantum-enhanced convolutions improve the performance of the model.

As explained above, the dataset used in the paper consists of spacial Fourier descriptors of skull contour. As was shown in other research [75], this brings enhancements to the forensic anthropology challenges, especially to sex, age, and ancestry estimation from unidentified crania. In the study [76] authors proposed applying machine learning algorithms to the task of gender classification from 3D models of skulls of the Greek population, involving Linear Discriminant Analysis, Decision Trees and Support Vector Machines.

Thus, our study unites the deep learning algorithms mentioned above and the power of FTs to tackle the challenge of sex estimation, which refers us to Fourier Neural Networks (FNN). As was shown in [77], FNN can bring significant improvements to the tasks of image recognition and language modeling. By using both MLP and CNN models within a FNN framework, our study explores sex determination from skeletal remains in anthropological research, presenting these tools as standard approaches to compare with our new methodologies.

3. Experimental setup

3.1. Parallel hybrid network with quantum depth infused layer

PHN is the first technique utilized in our study for the classification of cranial vault by gender. The architecture of the hybrid quantum model used in our work is presented in Fig. 2. Before entering the exact PHN layer, 1D Batch Normalization is applied to the input vector. Than this vector of dimension 64 comes to the input of both the classical and quantum parts of the PHN layer. The classical part consists of linear layers and activation functions between them (bottom rectangle "Classical layers" in Fig. 2). The input vector, after the first layer, is transformed into a vector of dimension 50. Then, the activation function $\mathrm{ReLU}(x)$:

$$\mathrm{ReLU}(x) = \max(0, x)$$

is applied to it, followed by another linear layer that transforms the vector to dimension 8.

The quantum part is represented by the QDI layer [48] (upper rectangle "Quantum Depth-Infused Layer" in Fig. 2). Each of the 64 features of the input vector before the quantum layer is encoded into 8 qubits (blue rectangles with R_Z in Fig. 2). The first 8 features are encoded by applying a rotation to each of the 8 qubits around the Z axis on the Bloch sphere, with the rotation angle being proportional to the corresponding value in the input vector. When we repeat the operations in the blue rectangle, we use other features: 9-16, then – 17-24, and so on. The number of repetitions of the operations in the blue rectangle is equal to the number of features divided by the number of qubits (in our case, 64 features / 8 qubits = 8 repetitions). To integrate the quantum layer into the neural network and adapt it to the data, variational layers are employed (purple rectangle in Fig. 2). In QDI, each variational layer consists of two parts: rotations with trainable parameters (in our case, rotations around the X axis) and subsequent CNOT (controlled not) operations. The formulas for the CNOT operation and rotations around the X and Z axes are presented below.

$$\mathrm{CNOT} = \begin{pmatrix} 1 & 0 & 0 & 0 \\ 0 & 1 & 0 & 0 \\ 0 & 0 & 0 & 1 \\ 0 & 0 & 1 & 0 \end{pmatrix}$$

$$R_x(\theta) = \begin{pmatrix} 1 & 0 & 0 \\ 0 & \cos\left(\frac{\theta}{2}\right) & -\sin\left(\frac{\theta}{2}\right) \\ 0 & \sin\left(\frac{\theta}{2}\right) & \cos\left(\frac{\theta}{2}\right) \end{pmatrix}$$

$$R_z(\theta) = \begin{pmatrix} \exp\left(-i\frac{\theta}{2}\right) & 0 \\ 0 & \exp\left(i\frac{\theta}{2}\right) \end{pmatrix}$$

The rotations act as quantum gates, modifying the states of qubits based on rotation parameters θ_i^j. CNOT operations further entangle the qubits within the quantum layer, generating a quantum superposition. During the measurement stage, all qubits, except the first one, undergo CNOT operations on the previous qubit. This process is followed by the Y measurement applied to all qubits, which converts information from the Hilbert space vector to a classical output of 8 neurons.

Following the described operations, the outputs from the classical and quantum layers are concatenated. The resulting vector then proceeds through the classical linear layer, which transforms it into a two-dimensional representation. Subsequently, the Softmax activation function:

$$\sigma(z_i) = \frac{e^{z_i}}{\sum_{j=1}^{K} e^{z_j}}$$

where z_i is the input for class i, and K is the total number of classes is applied, yielding a vector where the first component corresponds to the probability of belonging to class 0 (indicating male), and the second component corresponds to class 1 (indicating female). The class determination is performed by selecting the higher value of probability in the two-dimensional output vector.

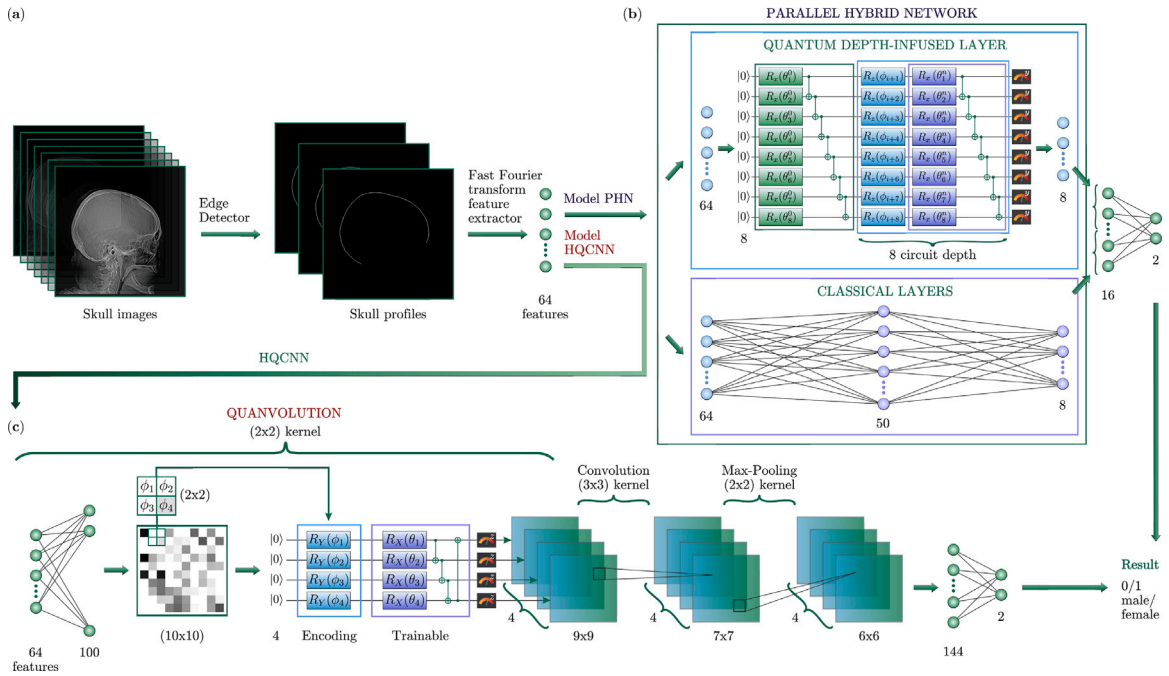

Fig. 2. **(a)** The dataset preprocessing steps before feeding the data to the model. **(b)–(c)** Architectures of the proposed models. The models are separate and not combined. **(b)** The architecture of PHN. **(c)** The architecture of HQCNN.

3.2. Classical counterpart: Multi-layer perceptron

As a classical counterpart we utilize MLP. The architecture of the model used in the study is similar to the architecture of the classic part of PHN (Fig. 2). The difference lies in the fact that a first linear transforms the input from a dimension of 64 to a dimension of 282, not 50. Following this, the hyperbolic tangent activation function

$$\tanh(x) = \frac{e^x - e^{-x}}{e^x + e^{-x}}$$

is applied. The final layer, similar to the PHN case, converts the output into a vector of dimension 2. It is noteworthy that the architecture of the neural network was optimized via Optuna [78]. Namely, the number of layers, the size of each layer, activation functions between layers, and the opportunity to add Batch Normalization layer before the layer was selected with the aim of accuracy maximization, incorporating 1000 Optuna trials. Moreover, after the architecture establishing, hyperparameters were optimized, specifically batch size, learning rate, epsilon, and betas parameters in Adam optimizer, utilizing the same tool.

The Batch Normalization layer at the beginning brings stability and robustness to the learning process of MLP model. The Softmax function is applied in the end to get two values that characterize the probability of belonging to each class as in the hybrid case.

3.3. Hybrid quantum convolutional network

Another hybrid model which we introduce is HQCNN. The architecture of this model is illustrated in Fig. 2. It begins with a 2D Batch Normalization layer, which normalizes the input vector, ensuring stable training and improving convergence like in previous models. After this, the input vector is transformed from a dimension of 64 to a dimension of 100 using a linear layer, followed by a ReLU activation function. This transformed vector is then reshaped into an image format with a size of 10×10. Subsequently, the image, after applying the 2D Batch Normalization layer, is fed into the quantum component — the quanvolutional layer.

In the QuanvLayer we employ a kernel just like those found in traditional convolutional layers, which processes segments of the input (in our case, 2×2 sized regions) to generate a new representation of the image. However, instead of a classical kernel, this model utilizes a VQC, as illustrated in Fig. 2.

We utilize a quantum circuit with four qubits, initializing each qubit in the ground state $|0\rangle$. We start with the encoding phase, where rotation around Y-axis based on features from the input is applied (represented by blue rectangles with R_Y in Fig. 2). Next is the variational phase, which employs 4 trainable parameters that determine the angles for rotations around X-axis for each qubit (shown as purple rectangles with R_X and parameters θ_i in Fig. 2). The last stage consists of a series of CNOT operations that entangle all qubits and create a quantum superposition. Each qubit undergoes a CNOT operation on the previous qubit, and the first qubit performs a CNOT operation with the last one. Finally, we perform a Z measurement on each qubit to obtain the vector with dimension 4. After processing the entire input with the described kernel, the resulting representation is a tensor with dimensions $9 \times 9 \times 4$.

After the quanvolutional layer a ReLU activation function utilized. The image then passes trough a classical convolutional layer with a kernel size of 3×3, resulting in an output shape of $7 \times 7 \times 4$. Another ReLU activation follows this step. Max pooling is then performed, yielding a final representation with dimensions of $6 \times 6 \times 4$. This tensor is reshaped into a 1D vector, resulting in a dimension of $6 \times 6 \times 4 = 144$. The Batch Normalization 1D layer is incorporated next for normalizing. After this we apply a linear layer to transform this vector into 2 output values. Finally, the Softmax function is used to present the probabilities for each class.

3.4. Classical counterpart: Convolutional neural network

To compare with the HQCNN model, we use a traditional CNN [79]. The architecture is similar to the hybrid model, but we use a regular convolutional layer instead of a quanvolutional layer. This traditional convolutional layer produce 4 output channels with a kernel which size is equal to 3 and parameter padding is equal to 2. After applying ReLU activation function, we downsample the output using max pooling, resulting in a tensor that measures $6 \times 6 \times 4$. Other layers are similar to those in the quantum model, with only the dimensions of inputs

Table 1
Comparison of model performance: accuracy, standard deviation, number of weights, and PR AUC.

Model	Accuracy, %	Std, %	Weights	PR AUC
PHN	**87.4**	**3.0**	**3892**	**0.953**
MLP	82.5	2.2	19158	0.943
HQCNN	83.4	2.2	7360	0.928
CNN	82.4	2.7	7384	0.923

and outputs differing. After the second convolutional layer and max pooling, we obtain a feature map of size $3 \times 3 \times 4$. The dimension of the vector entering the final linear layer is $3 \times 3 \times 4 = 36$. Finally, we apply the Softmax function to generate class probabilities as in previous cases.

3.5. Training and results

For our loss computation, we adopt the cross-entropy formula, which is applied to both the classical and hybrid models:

$$l = -\sum_{c=1}^{k} y_c \log p_c \tag{1}$$

Here, p_c symbolizes the predicted probability for a class, and y_c is a binary value, 0 or 1, designating whether an image corresponds to the predicted class, k denotes the total class count. The training process for each model is optimized using the Adam algorithm [80].

3.5.1. Parallel hybrid network vs. Multi-layer perceptron

To achieve the best accuracy for our PHN model, calculated as the number of correct answers on the test dataset divided by the size of that dataset, we utilized the architecture presented in Fig. 2. During the training process, both the MLP and PHN were trained for 40 epochs using the Adam optimizer. All hyperparameters including batch size, learning rate and Adam parameters were optimized with the Optuna optimizer [78].

The best accuracy achieved on the test dataset, that was determined through a cross-validation process with a 9: 1 splitting ratio, was $87.4 \pm 3.0\%$. This value was obtained by selecting the highest accuracy recorded during the full 40-epoch training for each model and then averaging these maximum values across all trained models. Notably, this result surpassed that of the MLP, which was calculated in the same manner and yielded an accuracy of $82.5 \pm 2.2\%$. This MLP accuracy is still slightly higher than the 82.25% reported in previous research conducted with this dataset [11].

In Fig. 3(a), the accuracy bars for the PHN and MLP models are presented. It is important to note that the architecture used for these models differs slightly from that shown in Fig. 2. Specifically, each series of CNOT operations in the PHN model concludes with an additional CNOT operation, where the last qubit serves as the control qubit and the first qubit functions as the target one.

This modification was implemented due to the fact that the model with the added CNOT operation demonstrated superior performance compared to the classical MLP model on reduced datasets, as illustrated in Fig. 3(a). However, when evaluating the entire dataset which includes 140 samples in the test set and 1240 samples in the training set, following a 1: 9 splitting ratio, the architecture shown in Fig. 2 achieved a higher accuracy of $87.4 \pm 3.0\%$ compared to $83.0 \pm 3.0\%$ for the model with the additional CNOT operation. Notably, the model with the highest accuracy on the entire dataset did not outperform the MLP on smaller training sets; their accuracies are comparable.

To obtain the results presented in Fig. 3(a), we utilized a fixed test set of 140 samples and trained 10 models on varying sizes of fixed training sets. Each model was subsequently evaluated using the same fixed test dataset. The presented bar chart confirms that the hybrid model is more stable as the standard deviation is as its standard deviation is consistently lower than that of the MLP. Additionally, it achieves higher accuracy than the classical one when applied to reduced datasets.

The described findings suggest that for situations with limited data, it may be advantageous to use the model with the last CNOT operation. Conversely, for larger datasets, the architecture depicted in Fig. 2 is more effective.

Notably, the classical model presented in our study incorporates a substantial 19,158 weights, underscoring the complexity required to effectively tackle our classification task. In contrast, the hybrid model stands out for its remarkable efficiency, utilizing only 3892 weights. The notable reduction in the number of weights highlights the computational efficacy of the hybrid model while maintaining competitive accuracy in addressing our classification task — sex determination based on the lateral shape of the calvarium.

To further investigate the efficiency of our hybrid model, we conducted an additional experiment in which we removed the quantum component from our architecture. In this setup, we trained a purely classical model that mirrored the classical part of the architecture depicted in Fig. 2. After training for 40 epochs, we achieved an accuracy of $79.4 \pm 5.4\%$. Notably, this architecture differs from the architecture of the best MLP itself, because it was searched with the Optuna optimizer as a part of the hybrid model. The results emphasize the important role of the quantum layer when combined with the MLP, demonstrating that integrating quantum and classical components in parallel can significantly enhance the model's capabilities. Additionally, to better understand the remaining misclassifications, we performed a brief error analysis on our best trained PHN (see Appendix for details), which reveals systematic mid-frequency shifts in the misclassified Fourier descriptors.

3.5.2. Hybrid quantum convolutional network vs. Convolutional neural network

For the other two models, HQCNN and CNN, we trained each for 50 epochs. All hyperparameters were also optimized using the Optuna optimizer [78]. To compare the performance of these models, we employed cross-validation with a 9:1 splitting ratio. The results showed that HQCNN achieved an accuracy of $83.4 \pm 2.2\%$, while CNN reached $82.4 \pm 2.7\%$. The accuracy values were calculated in the same manner as those for the previously described models. These findings underscore the potential advantages of utilizing quanvolutional layers in practical applications.

When comparing the number of trainable parameters between the models, we find that they are relatively close. The HQCNN model has 7360 parameters, while the CNN model has 7384. This small difference in the number of parameters highlights an important point: even though both models are nearly identical in terms of size, the HQCNN shows superior performance. This suggests that HQCNN is more efficient in utilizing its parameters to achieve better results.

All information about the models is summarized in Table 1. To evaluate the statistical significance of these results, we conducted two-sided Wilcoxon signed-rank tests on the cross validation accuracies of each model pair; the full procedure is detailed in Appendix. The tests confirm that the PHN model significantly outperforms MLP, HQCNN, and CNN ($p < 0.01$ between all pairs that include PHN), whereas HQCNN does not differ significantly from the classical baselines ($p > 0.05$).

Additionally, we have conducted an experiment to construct a precision–recall curve by varying the thresholds for all four models — MLP, PHN, HQCNN, and CNN. We selected the first component of the output vector as the probability of belonging to class 0. The curve which compares the models is presented in Fig. 3(b). Precise figures on the areas under those precision–recall curves can be seen on Table 1 (PR AUC). The results indicates that PHN outperforms MLP, demonstrating its greater suitability for imbalanced classification scenarios. Furthermore, the precision–recall curve for HQCNN also outperformed the classical CNN model, highlighting the effectiveness of hybrid models in addressing classification challenges.

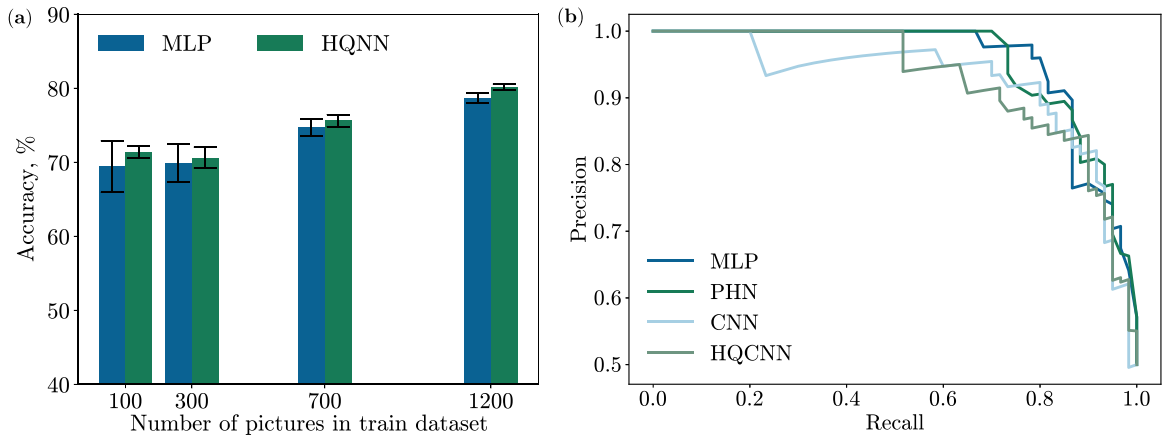

Fig. 3. **(a)** Bar chart showing the accuracy on the fixed test dataset and its deviation when trained on subsets of the training data with 100, 300, 700, and 1200 samples. Blue bars represent MLP performance, while green bars correspond to PHN. **(b)** The line graphs demonstrate precision–recall curves for the 4 models: MLP, PHN, CNN, and HQCNN, evaluated on the full test dataset.

3.5.3. Forward pass on the QPU

All models were trained using exact computation on a classical simulator provided by PennyLane [81]. The "lightning-qubit" backend was used to perform fast linear algebra calculations for simulating the evolution of quantum state vectors. To evaluate the PHN model — our top-performing model — on quantum hardware, we utilized IBM's quantum processing unit (QPU) [82], which leverages superconducting quantum technologies. In this study we used *ibm-brisbane*, a 127-qubit IBM Quantum Eagle processor.

We ran the forward pass of the best-trained PHN model on the QPU through the Qiskit SDK [83]. We took the best model from cross-validation and performed a forward pass on the part of the dataset marked as test. Each test sample's circuit was compiled using Qiskit's Transpiler (optimization level=3) to map logical qubits to the hardware coupling map and decompose gates into the native set. The number of shots was equal to 1000, and the test dataset included 140 items. The total quantum runtime was equal to 280 seconds. Without applying any error mitigation beyond Qiskit's defaults, the obtained result was 90.71%, which is slightly below the accuracy of the ideal simulator: 92.14% (the consideration of wrong samples is in Appendix). This result was expected due to shot noise and gate errors, but it still remains high, demonstrating that presented PHN model can be executed on contemporary quantum hardware with minimal loss in accuracy.

In summary, both hybrid models — PHN and HQCNN — outperform their classical counterparts across multiple criteria. The PHN achieves a 4.9% higher accuracy than the MLP (87.4% vs. 82.5%) with nearly five times fewer parameters (3,892 vs. 19,158), and shows superior generalization on reduced datasets. Similarly, the HQCNN surpasses the traditional CNN in accuracy (83.4% vs. 82.4%) while using a comparable number of parameters. Furthermore, hybrid models demonstrate better performance in terms of the area under the precision–recall curve, indicating greater robustness in imbalanced classification scenarios. Importantly, the PHN model was successfully executed on IBM's superconducting quantum processor, confirming the feasibility of running such hybrid architectures on existing quantum hardware. These results collectively highlight the advantages of integrating quantum components into classical neural architectures for forensic anthropology tasks.

4. Discussion

Machine learning has become an important tool across various fields, including medicine, finance, criminal justice, ballistics, entomology, and genetics. Its impact on forensic and physical anthropology is significant. Machine learning models helps identify subtle patterns in data and improves the accuracy, reliability, and efficiency of diagnostics, making it a valuable asset in advancing forensic anthropology.

Machine learning has demonstrated greater results than traditional methods across diverse forensic disciplines including forensic anthropology [84,85]. In a study related to image analysis deep learning model for diatom detection demonstrated increased efficiency and comparable accuracy to human experts [86]. In the field of forensic medicine authors used CNN to identify fatal hypothermia from post-mortem computed tomography (PMCT) images, achieving a maximum area under the ROC curve of 0.956. [87]. Another paper introduced a neural network that surpassed the Iris program in cause-of-death determination [88]. The next study presented a neural network that excelled in distinguishing marks on bones, outperforming taphonomy experts [89]. In forensic ballistics, the AI-based ensemble classifier developed by Savakar and Kannur demonstrated better results than traditional methods [90]. These examples highlight the potential of machine learning to enhance forensic analyses and surpass conventional approaches.

The studies mentioned above collectively demonstrate the capacity of machine learning models to assist forensic experts in addressing highly specific tasks. Moreover, these models can analyze and interpret vast amounts of data more efficiently than humans, positioning machine learning as a valuable tool for specialists.

An important aspect of our work is the evaluation of model performance using FT on images. Previous studies have indicated that applying FT can enhance model outcomes. For instance, one study highlights the benefits of FT in emotion detection tasks when working with two binary SVMs [91]. Another work demonstrates that using a basic Fourier feature mapping to transform input points allows MLP to learn high-frequency functions in low-dimensional problem domains, leading to improved results [92]. In a recent study, the performance of a CNN model in image classification was compared with and without FT preprocessing, and the results demonstrated a substantial improvement in classification accuracy when the transform was utilized [93]. These findings underscore the potential of FT as an effective feature extractor for our particular task.

In our study, we present HQNNs aimed at solving a specific applied problem in forensic and physical anthropology — sex determination based on the lateral shape of the calvarium. The novelty of our work lies in our pioneering application of quantum machine learning in the field of forensic and physical anthropology, with the results surpassing those achieved through classical methods. That models serve as a starting point for the development of a reliable and efficient computer system at the intersection of quantum computing and machine learning, acting as a valuable assistant for specialists in forensic and physical anthropology.

The presented hybrid models, along with its classical counterparts, underwent training on 1400 Fourier representations of lateral scout-view MDCT scanogram, all demonstrating high accuracy — exceeding 80%. This level of accuracy is comparable to that of an experienced specialist, highlighting the potential of machine learning models in the field of forensic and physical anthropology. Notably, in this particular task the PHN and MLP models outperformed both CNN and HQCNN.

The PHN model surpassed its classical counterpart in terms of accuracy. The PHN achieved an accuracy of $87.4 \pm 3.0\%$, while the MLP achieved an accuracy of $82.5 \pm 2.2\%$. This improvement plays a pivotal role in forensic anthropology, emphasizing the significance of precise results. Additionally, the slightly modified hybrid model displayed less variability and higher score in accuracy with a smaller datasets, indicating enhanced generalization ability.

Moreover, the substantial difference in the number of weights between the hybrid and classical models, precisely the number of weights of the best classic model is 4.92 times greater than that of the hybrid model, underscores the superior computational capacity of hybrid neural networks. The hybrid model's incorporation of a PHN layer effectively leveraged the advantages of both quantum and classical approaches through parallel data processing. The utilization of a QDI layer efficiently handled large input vectors. These outcomes showcase the prowess of hybrid neural networks in addressing forensic anthropology challenges, particularly in sex determination task.

A notable aspect of this study is the successful deployment of the best-trained PHN model on a QPU. The results obtained from the QPU run — 90.71% accuracy — were closely comparable to those from the classical simulation, which achieved 92.14%. This demonstrates that the hybrid model is not only effective in theory but also works well in practice when run on real quantum hardware.

Our study demonstrates that adding a quantum layer in parallel to the classical one enhances the model's capabilities. As it was shown, when we removed the quantum component from the HQNN model, the resulting accuracy was only $79.4 \pm 5.4\%$ which is 8% lower than the final accuracy of the hybrid model. We propose that the quantum layer, utilizing only 8 qubits and 64 trainable parameters, assists the classical layer in finding deeper minima in the landscape of the loss function.

Convolutional layers has also demonstrate great results. The HQCNN has shown superior performance compared to traditional CNNs. While the CNN achieved an accuracy of only $82.4 \pm 2.7\%$, the HQCNN showcased a more stable and higher accuracy of $83.4 \pm 2.2\%$. This improvement underscores the effectiveness of hybrid models over classical approaches. Furthermore, it highlights the promising potential of incorporating quanvolutional layers in practical applications.

As mentioned in the previous section, the number of weights in the CNN and HQCNN models are comparable, with CNN having a slightly higher count. Specifically, the classical model has 7384 weights, while the hybrid model has 7360, resulting in a difference of just 24 weights, or approximately 0.33%. Despite this marginal difference in complexity, Fig. 3(b) demonstrates that the hybrid model exhibits superior performance in terms of the area under the precision–recall curve. This indicates that HQCNN is more effective in handling imbalanced datasets compared to the CNN.

The overall results of our study highlight the value of hybrid quantum–classical architectures in forensic anthropology. Both presented HQNN models (PHN and HQCNN) outperformed their classical counterparts (MLP and CNN, respectively) across several key metrics, including accuracy and precision–recall characteristics. Moreover, the PHN model shows enhanced generalization and greater stability on reduced datasets compared to MLP. These improvements are especially relevant in real-world forensic settings, where datasets are often limited and imbalanced. In addition to their performance benefits, HQNNs offer reduced parameter complexity, and the PHN model demonstrated feasibility of execution on real quantum hardware. Together, these results support the integration of quantum-enhanced components into neural architectures for complex classification tasks in anthropology.

Beyond empirical performance, this work contributes to the growing body of research at the intersection of quantum computing and applied sciences. Our approach introduces quantum-enhanced learning to the specific domain of sex classification from cranial morphology — a task central to both physical and forensic anthropology. This study is among the first to apply hybrid quantum models to anthropological data. By bridging these two fields, we provide a proof-of-concept that demonstrates how quantum computing can support domain experts in solving high-stakes, data-sensitive classification problems.

These findings lay the groundwork for future systems that integrate quantum-enhanced architectures into computer-aided diagnosis tools used in forensic and archaeological contexts. In particular, such systems may assist anthropologists in analyzing incomplete or degraded skeletal remains, where automated support is most valuable. We believe this interdisciplinary direction can inspire further development of intelligent tools that augment expert decision-making under real-world constraints.

Limitations and future challenges

While our study demonstrates the potential of HQNNs in forensic anthropology, several limitations must be acknowledged. First, the dataset employed is relatively small, consisting of only 1400 samples. This fact may limit the generalizability of our models to broader or more heterogeneous populations, where greater morphological variability could affect the performance.

Another important limitation lies in the reliance on handcrafted features, specifically Fourier descriptors extracted from cranial contours. Although this method has proven effective [10], it introduces a degree of operator dependence in the preprocessing phase. Thus, our models rely on the user's choise of initial and final points of the cranial vault and the results are not completely reproducible.

Finally, the current deployment of HQNNs on real quantum hardware is constrained by technological limitations. The restricted number of available qubits, gate noise, and overall hardware instability impact both the scalability and the accuracy of hybrid models.

Future work could address these challenges by developing fully operator-independent feature extraction methods, such as integrating CNN-based automatic contour detection. As quantum hardware improves, scaling HQNNs to larger datasets and applying them to more complex forensic analyses will become possible. Moreover, future work should also take into account potential security concerns if HQNNs are to be used in applications involving sensitive information. While this is not a central issue in our current study, recent works have drawn attention to the fact that even advanced algorithms can be vulnerable during real-world implementation [94]. Security-focused strategies from recent research on compact implementations for modern processors [95], high-performance cryptographic architectures [96–98], and efficient cryptographic methods for resource-constrained applications [99] could guide the development of robust hybrid quantum–classical inference engines. Furthermore, incorporating general fault detection mechanisms inspired by proven fault-tolerant designs [100–103], alongside insights from medical device security research, would significantly enhance the resilience of HQNN systems against emerging security threats.

5. Conclusion

In conclusion, our study introduces hybrid models such as PHN and HQCNN as novel tools for addressing tasks in forensic anthropology. This new approach marks an important step forward in the field by combining the advantages of quantum computing and neural networks. We also investigate the effectiveness of presented models by leveraging FT as our feature extractor. Our results demonstrate that PHN and HQCNN outperform their classical counterparts in terms of accuracy of

sex classification. Specifically, PHN achieved the highest accuracy of $87.4 \pm 3.0\%$, surpassing the classical model's $82.5 \pm 2.2\%$, while HQCNN also demonstrated superior performance compared to the traditional CNN model. Compared to previous approaches applied to the same task and dataset, our hybrid models achieve better performance. In particular, the pattern recognition system based on classical neural networks described in [10] achieved an accuracy of 82.25%, which is lower than that of our best model and does not account for the evaluation on a reduced dataset—an aspect that was included in our research. Furthermore, we successfully deployed the best-trained PHN model on the QPU, achieving 90.71% accuracy, closely matching the 92.14% obtained from the classical simulation, demonstrating the practical possibility of running hybrid models on real quantum hardware. The improved performance of these models highlights the potential of HQNNs to enhance the accuracy and reliability of various forensic tasks.

Additionally, PHN exhibits greater stability and accuracy when working with smaller datasets. This is particularly important in anthropological research, where sample sizes are often limited. The reduced variability and consistent performance of PHN make it a good choice for forensic applications, leading to more reliable and accurate results.

A further improvement, which is beyond the scope of this paper as it is intrinsic to the preprocessing phase, would be the use of an automatic feature extraction algorithm, such as a convolutional neural network. The use of such an algorithm would make it possible to create a completely operator-independent tool, making the system even more robust than the current one, as the input features to the neural network would not be subject to the user's experience in selecting the initial and final points of the cranial vault to determine the initial contour from which features would be automatically extracted, but would be extracted automatically and always in the same way.

Future work directions may include:

- Developing a fully operator-independent system by integrating automatic feature extraction via CNNs directly from cranial scanograms.
- As quantum hardware advances, future work could focus on scaling our HQNNs to larger datasets and more complex forensic tasks, which could improve existing models' performance by increasing the number of qubits and operations in each VQC.
- The success of HQNNs on this dataset encourages extending them to the integration of multimodal data, such as 3D scans and genetic markers to enhance forensic diagnostics.

CRediT authorship contribution statement

Asel Sagingalieva: Writing – review & editing, Writing – original draft, Visualization, Software, Investigation. **Luca Lusnig:** Writing – review & editing, Writing – original draft, Investigation, Conceptualization. **Fabio Cavalli:** Writing – review & editing, Validation, Supervision, Investigation, Data curation. **Alexey Melnikov:** Writing – review & editing, Supervision, Project administration, Investigation.

Compliance with ethical standards

The research presented in this manuscript involved the use of skeletal remains, specifically calvarial profiles and their morphological data. All procedures were conducted in accordance with the relevant national and institutional guidelines for the ethical handling and study of human remains. No living human subjects were involved in this study, and thus no specific consent was required.

Funding

This research did not receive any specific grant from funding agencies in the public, commercial, or not-for-profit sectors.

Declaration of competing interest

None Declared.

Acknowledgments

We acknowledge Viacheslav Kuzmin for supporting the implementation of the forward pass on QPUs.

Appendix

A.1. ZX-Calculus

In this section, we thoroughly examine a presented quantum circuit named QDI that is shown in Fig. 2. We assess described circuit using ZX-calculus circuit reducibility.

The ZX-calculus serves as a powerful graphical language that enables the simplification and optimization of quantum circuits. By representing quantum circuits as "spiders" nodes — points connected by edges within a ZX diagram — this language allows circuits to be visualized and then streamlined through a process of graphical transformations based on ZX-calculus rules [104]. These transformations reduce the graph to an equivalent, optimized structure, thereby producing a more efficient quantum circuit configuration.

Simplification using ZX-calculus provides a metric for assessing circuit efficiency by comparing the number of parameters in the simplified form against the original. A lower parameter count indicates the removal of redundancies, leading to enhanced circuit performance. If no further reduction is possible, the circuit is deemed ZX-irreducible, meaning it has achieved an optimal level of trainable parameters without any superfluous elements [105].

In Fig. 4(a) the circuit before reduction can be observed. Fig. 4(b), in turn, demonstrates the ZX-representation after reduction. Despite the simplification process, the circuit retains all 72 initial parameters, confirming its ZX-irreducibility. This irreducible state indicates that no further parameter reduction is possible without compromising the circuit's functionality. Consequently, the circuit is deemed optimal, as each remaining parameter contributes directly to its operation, leaving no redundancies.

The ZX-calculus algorithm confirms that QDI operates with maximal efficiency, as no parameters are found to be redundant. This outcome suggests a high level of optimization within the model. However, to achieve a more comprehensive evaluation of circuit performance, other assessment metrics should be considered.

A.2. Fisher information

The Fisher Information Matrix (FIM) is a crucial metric used to evaluate the trainability of machine learning models, especially HQNNs [106]. In supervised learning, the FIM captures how sensitive the model's output distribution is to changes in its parameters. This sensitivity provides insight into the significance of each parameter during training [107]. High values on the diagonal of the FIM indicate that a parameter significantly affects the model's output, suggesting its importance. Conversely, low off-diagonal values reflect minimal correlation between parameters, which indicates that the parameters work independently and reduces redundancy in the model.

In QML, Fisher analysis is particularly valuable for identifying and mitigating the *barren plateau* problem [108]. Barren plateaus occur when gradients become vanishingly small, making it difficult to train the model effectively as the number of qubits increases. The eigenvalue spectrum of the FIM is used to detect this issue: if many eigenvalues are close to zero, it indicates that some parameters are not contributing to the learning process, reducing the model's trainability.

In Fig. 5(a) one can observe the FIM analysis of the QDI cirtuit utilized in our study. The heatmap shows the following:

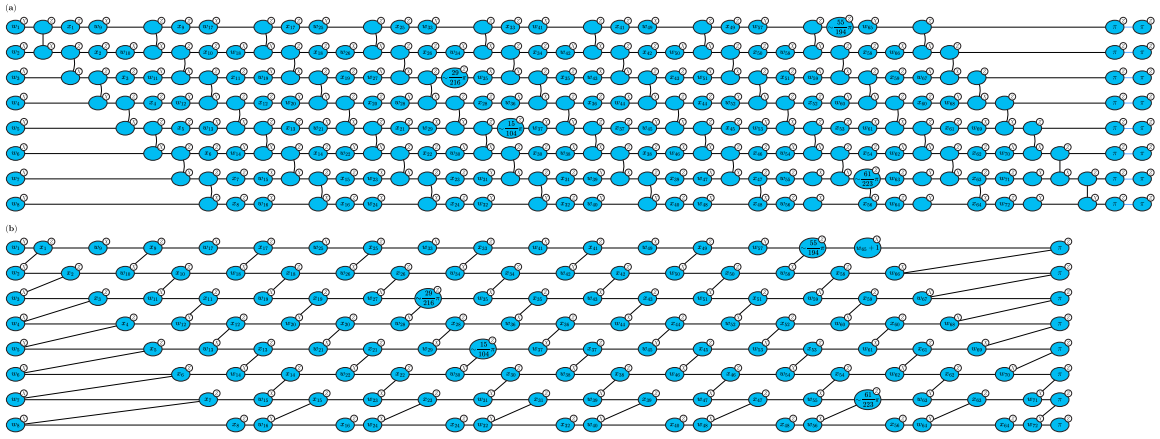

Fig. 4. ZX analysis of the QDI circuit utilized in the study. **(a)** Initial circuit before reduction. **(b)** Optimized circuit after ZX reduction.

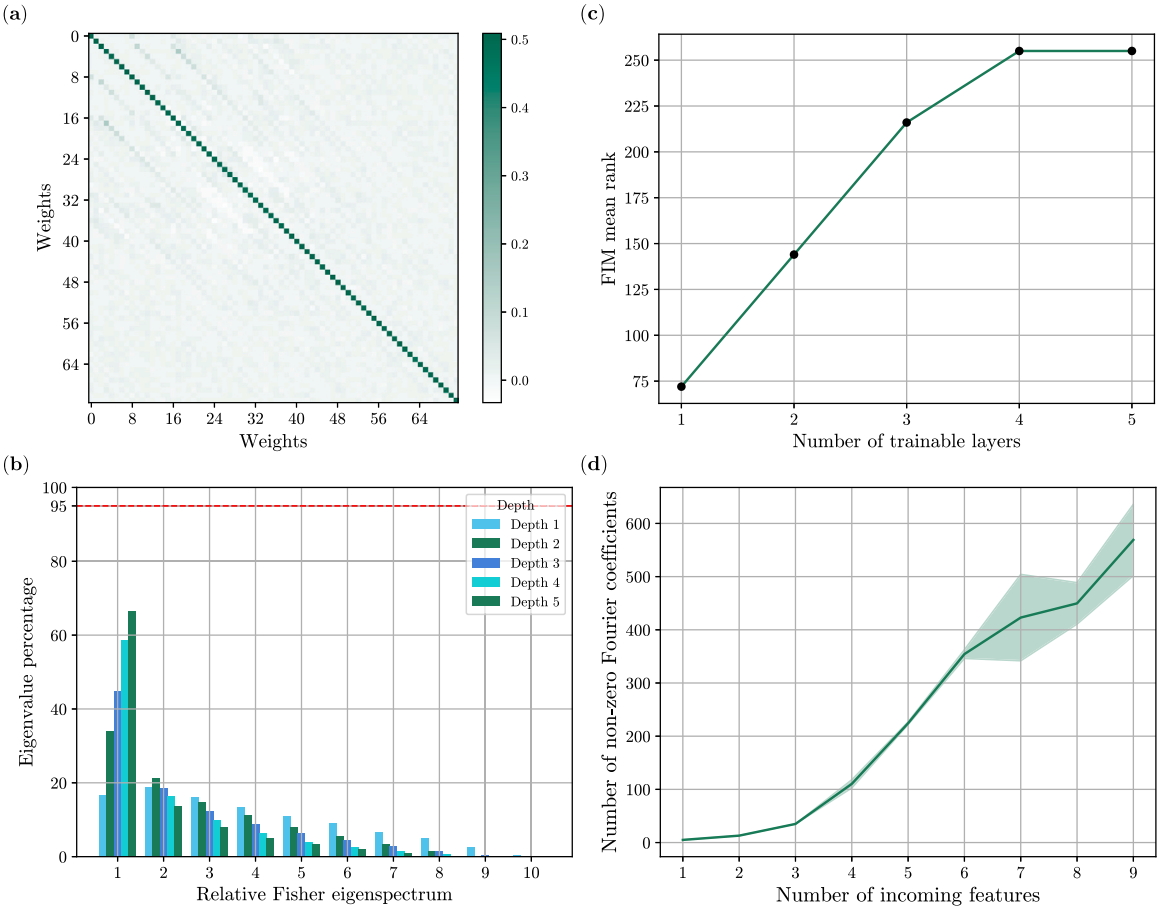

Fig. 5. Fisher and Fourier analysis for the QDI circuit, utilized in the study. **(a)** Average Fisher Information Matrix (FIM), showing strong diagonal dominance and minimal off-diagonal interaction, indicating well-distributed gradients across parameters. **(b)** Relative Fisher eigenspectrum, where the high-frequency distribution of eigenvalues suggests excellent trainability. In the QDI circuit utilized in the study parameter depth is equal to 1. **(c)** FIM rank analysis showing that the QDI circuit with depth = 1 is expressive but not overparameterized. **(d)** Dependence of the number of non-zero Fourier coefficients on the number of input features for the smaller QDI analogy.

1. *Diagonal Dominance*: The FIM exhibits high values along the diagonal, which implies that most parameters have a significant influence on the model's output distribution. This diagonal dominance indicates minimal redundancy and high individual parameter importance, suggesting that the parameters are optimized for effective learning without unnecessary complexity.
2. *Low Off-Diagonal Elements*: The off-diagonal elements are close to zero, indicating minimal correlation between parameters. This lack of correlation implies that the parameters operate largely independently, enhancing the trainability of the model. Minimal parameter interaction ensures that adjusting one parameter has little impact on others, which simplifies the optimization landscape and can speed up convergence during training.

The structure of the FIM, characterized by strong diagonal elements and low eigenvalue degeneracy, suggests that the model is highly trainable and less prone to barren plateaus.

The graph in Fig. 5(b) illustrates the trainability analysis of quantum circuits with varying depths, focusing on the distribution of the Fisher information eigenvalue spectrum. This distribution is essential in understanding how different circuit depths affect the model's ability to learn effectively. Notably, Depth 1 shows a more balanced spread of eigenvalues, suggesting a favorable training landscape with reduced risk of barren plateau phenomenon where the optimization landscape becomes flat, hindering training progress. The red dashed line at the 95% level serves as a threshold; if the proportion of small eigenvalues exceeds this line, trainability issues may arise. As depth increases, eigenvalues cluster more heavily at lower values, indicating a higher likelihood of barren plateaus and greater difficulty in training. Therefore, a circuit depth of 1 is particularly advantageous, offering a well-conditioned training environment that promotes effective learning.

The graph in Fig. 5(c) illustrates the overparameterization analysis by showing the mean rank of the FIM as a function of the number of trainable layers. With a single trainable layer, we observe a balanced configuration where the FIM rank is sufficient to capture the necessary model expressivity without reaching the overparameterization regime. This single-layer setup provides an optimal balance, ensuring the model is both efficient and trainable without the need for excessive parameters.

A.3. Fourier accessibility

Fourier analysis is a useful method for understanding how expressive quantum circuits can be, especially in quantum machine learning. It allows us to represent quantum models as partial Fourier series, where the frequencies come from data encoding gates, and the coefficients are controlled by the trainable parts of the circuit. This helps to identify what types of functions a quantum circuit can approximate. For example, repeating encoding gates multiple times allows the circuit to access more frequencies, making it possible to approximate more complex functions [109].

Data encoding plays a key role in defining the range of frequencies a quantum circuit can use. Repeating the encoding, either in sequence or in parallel, increases the number of frequencies the circuit can handle, improving its expressivity. This makes it important to carefully design the encoding strategy, as it directly affects what the model can learn. Additionally, the trainable parts of the circuit adjust the Fourier coefficients, further improving the model's capacity.

In our QDI setup, we faced challenges in applying Fourier analysis directly to an 8-qubit QDI circuit with 64 encoding features, as this would require calculating approximately 3^{64} Fourier coefficients, which is computationally infeasible. To address this, we conducted an experiment using a scaled-down version of the circuit. This reduced model consisted of 3 qubits and maintained the same QDI architecture as the 8-qubit circuit shown in Fig. 2. For this 3-qubit setup, we incrementally increased the number of input features from 1 to 9 and computed the number of non-zero Fourier coefficients in the truncated Fourier series.

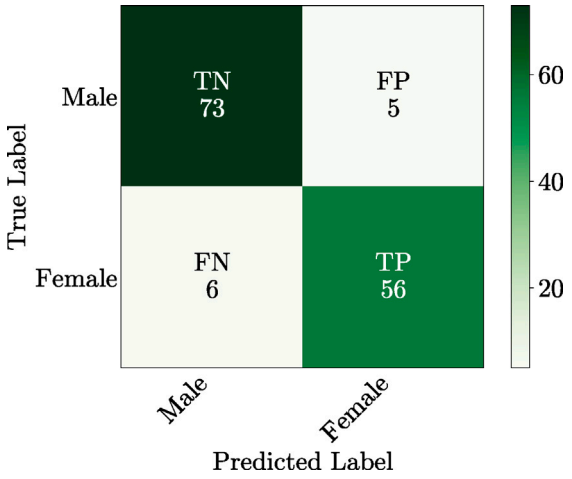

Fig. 6. Confusion matrix for the PHN model on the validation fold. Each cell is annotated with the count and label (TN: true negatives, FP: false positives, FN: false negatives, TP: true positives) for Male (0) vs. Female (1) classification.

The results, as depicted in Fig. 5(d), demonstrate a clear growth in the number of non-zero Fourier coefficients as the number of input features increases. This indicates that the expressivity of the circuit expands with more features, supporting the hypothesis that the larger 8-qubit QDI circuit with 64 features is likely capable of generating a rich and diverse Fourier spectrum. These findings provide confidence in the circuit's potential to approximate complex functions effectively.

A.4. Error analysis

We performed a detailed error analysis of our top-performing model on the same validation subset later executed on the QPU. First, we constructed the confusion matrix (Fig. 6), which shows 11 total misclassifications: 5 false positives (male predicted as female) and 6 false negatives (female predicted as male).

Raw counts and visual inspection alone cannot explain these errors, so we compared the average log-spectra of its 64-dimensional Fourier inputs for each outcome (Fig. 7). A global trend emerges: correctly predicted female samples have slightly higher mid-frequency amplitudes than correctly predicted male samples. We observed clear shifts in the mean misclassification curves: false positives (male samples predicted as female) are shifted upward, consistent with a prediction of "1", while false negatives (female samples predicted as male) are shifted downward, consistent with a prediction of "0". However, this mid-frequency shift does not fully determine individual predictions. In particular, samples whose spectra oscillate around the mean or even those whose amplitudes shift toward the male mean yet are classified as female demonstrate that the model relies on more complex, higher-order relationships within the descriptor space. While the average-spectrum shift is a useful overarching observation, the actual decision boundaries of the network reflect more subtle feature interactions that are not obvious to the human eye.

Finally, when running on the QPU, only two samples were misclassified. In both cases, the pre-QPU softmax probabilities were very close to 0.5 (0.4983 vs. 0.5017 and 0.5082 vs. 0.4918), so device noise tipped the decision over the threshold (to 0.5004 vs. 0.4996 and 0.4615 vs. 0.5385). This suggests that on noisy hardware only samples with near-equivocal scores are at risk. If stable QPU performance is required, one should either increase the model's confidence margin or flag low-confidence predictions for manual review.

Table 2
Wilcoxon signed-rank test results for tenfold cross validation accuracies, where r is the rank-based effect size and d is Cohen's d.

Pair	Wilcoxon test (W)	p-value	Significant (p<0.05)	Effect size r	Cohen's d
PHN vs MLP	3.0	0.0098	Yes	0.79	1.339
PHN vs CNN	2.0	0.0059	Yes	0.822	1.152
HQCNN vs MLP	5.0	0.0684	No	0.725	−0.621
HQCNN vs CNN	19.5	0.4922	No	0.258	0.282
PHN vs HQCNN	5.0	0.0195	Yes	0.725	1.031

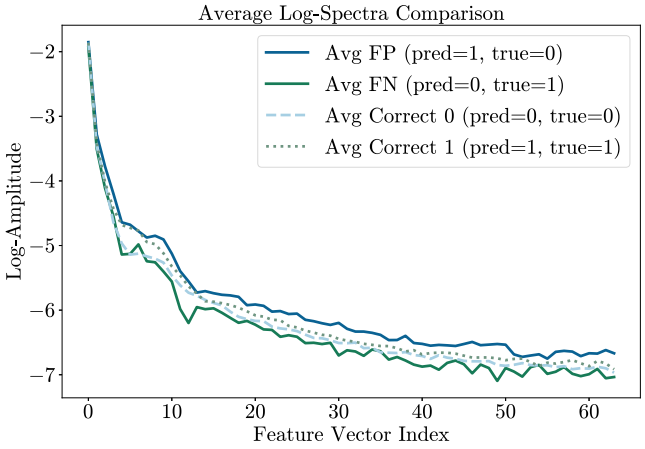

Fig. 7. Amplitudes of the input vector.

A.5. Statistical comparison

To estimate the significance of achieved results we have incorporated additional statistical analysis based on the accuracy achieved from 10-fold cross-validation. We used the two-sided Wilcoxon signed-rank test, a nonparametric method for paired data that assesses whether the median of differences between two related samples is zero [110, 111]. Unlike the paired t-test, it does not require the differences to be normally distributed.

For each pair of models, the following metrics are reported in Table 2:

- **Wilcoxon test** (W)
  The Wilcoxon signed-rank statistic, defined as the smaller of the sums of positive and negative ranks of the differences (the lower value corresponds to the higher statistical difference.
- **p-value**
  The probability of observing a test statistic at least as extreme as W under the null hypothesis of no difference.
- **Significant**
  "Yes" if $p < 0.05$, indicating rejection of the null hypothesis at the 5% level.
- **Effect size** r
  Calculated as $r = |Z|/\sqrt{N}$, where Z is the standardized test statistic and N is the number of paired observations; thresholds of 0.1, 0.3, and 0.5 indicate small, medium, and large effects.
- **Cohen's** d
  The mean of the paired differences divided by their standard deviation, with $|d| > 0.8$ conventionally interpreted as a large effect [112].

The results in Table 2 show that the PHN model achieves statistically higher accuracy than MLP, HQCNN, and CNN, with all three pairwise p-values below 0.01 and large effect sizes ($r > 0.7$, $|d| > 1.0$). By contrast, comparisons between HQCNN and the classical models yield $p > 0.05$ and small-to-medium effects, indicating no reliable difference. These findings confirm that PHN's advantage is both statistically significant and practically substantial, whereas HQCNN performs on par with its classical counterparts.

References

[1] Iscan MY, Steyn M. The human skeleton in forensic medicine. Charles C Thomas Publisher; 2013.
[2] Spradley MK, Jantz RL. Sex estimation in forensic anthropology: skull versus postcranial elements. J Forensic Sci 2011;56(2):289–96. http://dx.doi.org/10.1111/j.1556-4029.2010.01635.x.
[3] Ogawa Y, Imaizumi K, Miyasaka S, Yoshino M. Discriminant functions for sex estimation of modern Japanese skulls. J Forensic Leg Med 2013;20(4):234–8. http://dx.doi.org/10.1016/j.jflm.2012.09.023.
[4] Rogers TL. Determining the sex of human remains through cranial morphology. J Forensic Sci 2005;50(3):JFS2003385. http://dx.doi.org/10.1520/JFS2004014.
[5] Hsiao T-H, Tsai S-M, Chou S-T, Pan J-Y, Tseng Y-C, et al. Sex determination using discriminant function analysis in children and adolescents: a lateral cephalometric study. Int J Legal Med 2010;124:155–60. http://dx.doi.org/10.1007/S00414-009-0412-1.
[6] Ramsthaler F, Kettner M, Gehl A, Verhoff M. Digital forensic osteology: morphological sexing of skeletal remains using volume-rendered cranial CT scans. Forensic Sci Int 2010;195(1–3):148–52. http://dx.doi.org/10.1016/j.forsciint.2009.12.010.
[7] Luo L, Wang M, Tian Y, Duan F, Wu Z, et al. Automatic sex determination of skulls based on a statistical shape model. Comput Math Methods Med 2013;2013. http://dx.doi.org/10.1155/2013/251628.
[8] Calder J, Coil R, Melton JA, Olver PJ, Tostevin G, et al. Use and misuse of machine learning in anthropology. IEEE BITS Inf Theory Mag 2022;2(1):102–15. http://dx.doi.org/10.1109/MBITS.2022.3205143.
[9] Del Bove A, Veneziano A. A Generalised Neural Network Model to Estimate Sex from Cranial Metric Traits: A Robust Training and Testing Approach. Appl Sci 2022;12(18):9285. http://dx.doi.org/10.3390/app12189285.
[10] Cavalli F, Lusnig L, Trentin E. Use of pattern recognition and neural networks for non-metric sex diagnosis from lateral shape of calvarium: an innovative model for computer-aided diagnosis in forensic and physical anthropology. Int J Legal Med 2017;131(3):823–33. http://dx.doi.org/10.1007/s00414-016-1439-8.
[11] Trentin E, Lusnig L, Cavalli F. Parzen neural networks: Fundamentals, properties, and an application to forensic anthropology. Neural Netw 2018;97:137–51. http://dx.doi.org/10.1016/j.neunet.2017.10.002.
[12] Biamonte J, Wittek P, Pancotti N, Rebentrost P, Wiebe N, et al. Quantum machine learning. Nature 2017;549(7671):195–202. http://dx.doi.org/10.1038/nature23474.
[13] Melnikov A, Kordzanganeh M, Alodjants A, Lee R-K. Quantum machine learning: from physics to software engineering. Adv Phys: X 2023;8(1):2165452. http://dx.doi.org/10.1080/23746149.2023.2165452.
[14] Schuld M, Fingerhuth M, Petruccione F. Implementing a distance-based classifier with a quantum interference circuit. Europhys Lett 2017;119(6):60002. http://dx.doi.org/10.1209/0295-5075/119/60002.
[15] Kordzanganeh M, Buchberger M, Kyriacou B, Povolotskii M, Fischer W, et al. Benchmarking Simulated and Physical Quantum Processing Units Using Quantum and Hybrid Algorithms. Adv Quantum Technol 2023;6(8). http://dx.doi.org/10.1002/qute.202300043.
[16] Nixon M, Aguado AS. Feature extraction and image processing. Oxford: Elsevier; 2008.
[17] Schalkoff RJ. Digital image processing and computer vision: an introduction to theory and implementations. John Wiley & Sons, Inc.; 1989.
[18] Canny J. A computational approach to edge detection. IEEE Trans Pattern Anal Mach Intell 1986;6:679–98. http://dx.doi.org/10.1109/TPAMI.1986.4767851.
[19] Davies ER. Machine vision: theory, algorithms, practicalities. Elsevier; 2004.
[20] Zhang D, Lu G, et al. A comparative study on shape retrieval using Fourier descriptors with different shape signatures. J Vis Commun Image Represent 2001;1.
[21] Vishnu VK, Rajput DS. A review on the significance of machine learning for data analysis in big data. Jordanian J Comput Inf Technol 2020;6(1). http://dx.doi.org/10.5455/jjcit.71-1564729835.
[22] Vaswani A, Shazeer N, Parmar N, Uszkoreit J, Llion Jones others s. Attention is all you need. 2023, http://dx.doi.org/10.48550/arXiv.1706.03762, arXiv preprint arXiv:1706.03762.
[23] Khanagar SB, Vishwanathaiah S, Naik S, Al-Kheraif AA, Divakar DD, et al. Application and performance of artificial intelligence technology in forensic odontology–a systematic review. Leg Med 2021;48:101826. http://dx.doi.org/10.1016/j.legalmed.2020.101826.

[24] Mauer MAd, Well EJ-v, Herrmann J, Groth M, Morlock MM, et al. Automated age estimation of young individuals based on 3D knee MRI using deep learning. Int J Legal Med 2021;135(2):649–63. http://dx.doi.org/10.1007/s00414-020-02465-z.

[25] Bewes J, Low A, Morphett A, Pate FD, Henneberg M. Artificial intelligence for sex determination of skeletal remains: Application of a deep learning artificial neural network to human skulls. J Forensic Leg Med 2019;62:40–3. http://dx.doi.org/10.1016/j.jflm.2019.01.004.

[26] Kuha A, Ackermann J, Junno J-A, Oettlé A, Oura P. Deep learning in sex estimation from photographed human mandible using the human osteological research collection. Leg Med 2024;70:102476. http://dx.doi.org/10.1016/j.legalmed.2024.102476.

[27] Oura P, Junno J-A, Hunt D, Lehenkari P, Tuukkanen J, et al. Deep learning in sex estimation from knee radiographs – a proof of concept study utilizing the terry anatomical collection. Leg Med 2023;61:102211. http://dx.doi.org/10.1016/j.legalmed.2023.102211.

[28] da Silva RLB, Yang S, Kim D, Kim JH, Lim S-H, et al. Automatic segmentation and classification of frontal sinuses for sex determination from CBCT scans using a two-stage anatomy-guided attention network. Sci Rep 2024;14(1):11750. http://dx.doi.org/10.1038/s41598-024-62211-y.

[29] Schuld M, Sinayskiy I, Petruccione F. An introduction to quantum machine learning. Contemp Phys 2015;56(2):172–85. http://dx.doi.org/10.1080/00107514.2014.964942.

[30] Forcer TM, Hey AJ, Ross D, Smith PG. Superposition, entanglement and quantum computation. Quantum Inf Process 2002;2(2):97–116. http://dx.doi.org/10.26421/QIC2.2-1.

[31] Ogur B, Yilmaz I. The effect of superposition and entanglement on hybrid quantum machine learning for weather forecasting.. Quantum Inf Comput 2023;23(3&4):181–94. http://dx.doi.org/10.26421/QIC23.3-4-1.

[32] Rebentrost P, Mohseni M, Lloyd S. Quantum support vector machine for big data classification. Phys Rev Lett 2014;113(13):130503. http://dx.doi.org/10.1103/PhysRevLett.113.130503.

[33] Schuld M, Killoran N. Quantum machine learning in feature Hilbert spaces. Phys Rev Lett 2019;122(4):040504. http://dx.doi.org/10.1103/PhysRevLett.122.040504.

[34] Wu Y, Wu B, Wang J, Yuan X. Quantum phase recognition via quantum kernel methods. Quantum 2023;7:981. http://dx.doi.org/10.22331/q-2023-04-17-981.

[35] Schnabel J, Roth M. Quantum kernel methods under scrutiny: A benchmarking study. Quantum Mach Intell 2025;7(1):58. http://dx.doi.org/10.1007/s42484-025-00273-5.

[36] Zhao R-X, Shi J, Li X. Qksan: A quantum kernel self-attention network. IEEE Trans Pattern Anal Mach Intell 2024. http://dx.doi.org/10.1109/TPAMI.2024.3434974.

[37] Cong I, Choi S, Lukin MD. Quantum convolutional neural networks. Nat Phys 2019;15(12):1273–8. http://dx.doi.org/10.1038/s41567-019-0648-8.

[38] Chen G, Chen Q, Long S, Zhu W, Yuan Z, Wu Y. Quantum convolutional neural network for image classification. Pattern Anal Appl 2023;26(2):655–67. http://dx.doi.org/10.1007/s10044-022-01113-z.

[39] Sun Y, Li D, Xiang Q, Yuan Y, Hu Z, Hua X, Jiang Y, Zhu Y, Fu Y. Scalable quantum convolutional neural network for image classification. Phys A 2025;657:130226. http://dx.doi.org/10.1016/j.physa.2024.130226.

[40] McClean JR, Boixo S, Smelyanskiy VN, Babbush R, Neven H. Barren plateaus in quantum neural network training landscapes. Nat Commun 2018;9(1):4812. http://dx.doi.org/10.1038/s41467-018-07090-4.

[41] Wang S, Fontana E, Cerezo M, Sharma K, Sone A, et al. Noise-induced barren plateaus in variational quantum algorithms. Nat Commun 2021;12(1):6961. http://dx.doi.org/10.1038/s41467-021-27045-6.

[42] Aaronson S, Chen L. Complexity-Theoretic Foundations of Quantum Supremacy Experiments. 2016, http://dx.doi.org/10.48550/arXiv.1612.05903, arXiv preprint arXiv:1612.05903.

[43] Skolik A, McClean JR, Mohseni M, Van Der Smagt P, Leib M. Layerwise learning for quantum neural networks. Quantum Mach Intell 2021;3:1–11. http://dx.doi.org/10.1007/s42484-020-00036-4.

[44] Cerezo M, Sone A, Volkoff T, Cincio L, Coles PJ. Cost function dependent barren plateaus in shallow parametrized quantum circuits. Nat Commun 2021;12(1):1791. http://dx.doi.org/10.1038/s41467-021-21728-w.

[45] Ortiz Marrero C, Kieferová M, Wiebe N. Entanglement-induced barren plateaus. PRX Quantum 2021;2(4):040316. http://dx.doi.org/10.1103/PRXQuantum.2.040316.

[46] Grant E, Wossnig L, Ostaszewski M, Benedetti M. An initialization strategy for addressing barren plateaus in parametrized quantum circuits. Quantum 2019;3:214. http://dx.doi.org/10.22331/q-2019-12-09-214.

[47] Wang S, Fontana E, Cerezo M, Sharma K, Sone A, Cincio L, Coles PJ. Noise-induced barren plateaus in variational quantum algorithms. Nat Commun 2021;12(1):6961. http://dx.doi.org/10.1038/s41467-021-27045-6.

[48] Sagingalieva A, Kordzanganeh M, Kenbayev N, Kosichkina D, Tomashuk T, Melnikov A. Hybrid quantum neural network for drug response prediction. Cancers 2023;15(10):2705. http://dx.doi.org/10.3390/cancers15102705.

[49] Perelshtein M, Sagingalieva A, Pinto K, Shete V, et al. Practical application-specific advantage through hybrid quantum computing. 2022, http://dx.doi.org/10.48550/arXiv.2205.04858, arXiv preprint arXiv:2205.04858.

[50] Riaz F, Abdulla S, Suzuki H, Ganguly S, Deo RC, et al. Accurate image multi-class classification neural network model with quantum entanglement approach. Sensors 2023;23(5):2753. http://dx.doi.org/10.3390/s23052753.

[51] Saggio V, Asenbeck BE, Hamann A, Strömberg T, Schiansky P, et al. Experimental quantum speed-up in reinforcement learning agents. Nature 2021;591(7849):229–33. http://dx.doi.org/10.1038/s41586-021-03242-7.

[52] Anoshin M, Sagingalieva A, Mansell C, Zhiganov D, Shete V, Pflitsch M, et al. Hybrid quantum cycle generative adversarial network for small molecule generation. IEEE Trans Quantum Eng 2024;5:2500514. http://dx.doi.org/10.1109/TQE.2024.3414264.

[53] Pistoia M, Ahmad SF, Ajagekar A, Buts A, Chakrabarti S, et al. Quantum machine learning for finance ICCAD special session paper. In: 2021 IEEE/ACM international conference on computer aided design. ICCAD, IEEE; 2021, p. 1–9. http://dx.doi.org/10.1109/ICCAD51958.2021.9643469.

[54] Sagingalieva A, Komornyik S, Senokosov A, Joshi A, Sedykh A, Mansell C, et al. Photovoltaic power forecasting using quantum machine learning. 2023, http://dx.doi.org/10.48550/arXiv.2312.16379, arXiv preprint arXiv:2312.16379.

[55] Sedykh A, Podapaka M, Sagingalieva A, Pinto K, Pflitsch M, Melnikov A. Hybrid quantum physics-informed neural networks for simulating computational fluid dynamics in complex shapes. Mach Learn: Sci Technol 2024;5(2):025045. http://dx.doi.org/10.1088/2632-2153/ad43b2.

[56] Haboury N, Kordzanganeh M, Schmitt S, Joshi A, Tokarev I, et al. A supervised hybrid quantum machine learning solution to the emergency escape routing problem. 2023, http://dx.doi.org/10.48550/arXiv.2307.15682, arXiv preprint arXiv:2307.15682.

[57] Nannicini G. Performance of hybrid quantum-classical variational heuristics for combinatorial optimization. Phys Rev E 2019;99:013304. http://dx.doi.org/10.1103/PhysRevE.99.013304.

[58] Li W, Chu P-C, Liu G-Z, Tian Y-B, Qiu T-H, et al. An image classification algorithm based on hybrid quantum classical convolutional neural network. Quantum Eng 2022;2022(1):5701479. http://dx.doi.org/10.1155/2022/5701479.

[59] Lusnig L, Sagingalieva A, Surmach M, Protasevich T, Michiu O, McLoughlin J, et al. Hybrid quantum image classification and federated learning for hepatic steatosis diagnosis. Diagnostics 2024;14(5):558. http://dx.doi.org/10.3390/diagnostics14050558.

[60] Rao GE, Rajitha B, Srinivasu PN, Ijaz MF, Woźniak M. Hybrid framework for respiratory lung diseases detection based on classical CNN and quantum classifiers from chest X-rays. Biomed Signal Process Control 2024;88:105567. http://dx.doi.org/10.1016/j.bspc.2023.105567.

[61] Yu K, Chakraborty C, Xu D, Zhang T, Zhu H, Alfarraj O, et al. Hybrid quantum classical optimization for low-carbon sustainable edge architecture in RIS-assisted AIoT healthcare systems. IEEE Internet Things J 2024. http://dx.doi.org/10.1109/JIOT.2024.3399234.

[62] Mazumdar H, Chakraborty C, Venkatakrishnan SB, Kaushik A, Gohel HA. Quantum-inspired heuristic algorithm for secure healthcare prediction using blockchain technology. IEEE J Biomed Heal Informatics 2023;28(6):3371–8. http://dx.doi.org/10.1109/JBHI.2023.3304326.

[63] Xiang Q, Li D, Hu Z, Yuan Y, Sun Y, Zhu Y, Fu Y, Jiang Y, Hua X. Quantum classical hybrid convolutional neural networks for breast cancer diagnosis. Sci Rep 2024;14(1):24699. http://dx.doi.org/10.1038/s41598-024-74778-7.

[64] Ray A, Madan D, Patil S, Pati P, Rapsomaniki M, Kohlakala A, et al. Hybrid quantum-classical graph neural networks for tumor classification in digital pathology. In: 2024 IEEE international conference on quantum computing and engineering. QCE, vol. 1, IEEE; 2024, p. 1611–6. http://dx.doi.org/10.1109/QCE60285.2024.00188.

[65] Kordzanganeh M, Kosichkina D, Melnikov A. Parallel hybrid networks: an interplay between quantum and classical neural networks. Intell Comput 2023;2:0028. http://dx.doi.org/10.34133/icomputing.0028.

[66] Kurkin A, Hegemann J, Kordzanganeh M, Melnikov A. Forecasting steam mass flow in power plants using the parallel hybrid network. Eng Appl Artif Intell 2025;160:111912. http://dx.doi.org/10.1016/j.engappai.2025.111912.

[67] Senokosov A, Sedykh A, Sagingalieva A, Kyriacou B, Melnikov A. Quantum machine learning for image classification. Mach Learn: Sci Technol 2024;5(1):015040. http://dx.doi.org/10.1088/2632-2153/ad2aef.

[68] Henderson M, Shakya S, Pradhan S, Cook T. Quanvolutional neural networks: powering image recognition with quantum circuits. Quantum Mach Intell 2020;2(1):2. http://dx.doi.org/10.1007/s42484-020-00012-y.

[69] Alam M, Kundu S, Topaloglu RO, Ghosh S. Quantum-classical hybrid machine learning for image classification. In: 2021 IEEE/ACM international conference on computer aided design. ICCAD, IEEE; 2021, p. 1–7. http://dx.doi.org/10.1109/ICCAD51958.2021.9643516.

[70] Song Y, Li J, Wu Y, Qin S, Wen Q, Gao F. A resource-efficient quantum convolutional neural network. Front Phys 2024;12:1362690. http://dx.doi.org/10.3389/fphy.2024.1362690.

[71] Venkatesh K, Naik KJ, Shankar A. Quantum convolution neural network for multi-nutrient detection and stress identification in plant leaves. Multimedia Tools Appl 2024;83(24):65663–85. http://dx.doi.org/10.1007/s11042-023-17992-1.

[72] Shen F, Liu J. QFCNN: Quantum Fourier convolutional neural network. 2021, http://dx.doi.org/10.48550/arXiv.2106.10421, arXiv preprint arXiv:2106.10421.
[73] Rumelhart DE, Hinton GE, Williams RJ. Learning representations by back-propagating errors. Nature 1986;323(6088):533–6. http://dx.doi.org/10.1038/323533a0.
[74] Younesi A, Ansari M, Fazli M, Ejlali A, Shafique M, Henkel J. A comprehensive survey of convolutions in deep learning: Applications, challenges, and future trends. IEEE Access 2024;12:41180–218. http://dx.doi.org/10.1109/ACCESS.2024.3376441.
[75] Caple J, Byrd J, Stephan CN. Elliptical Fourier analysis: fundamentals, applications, and value for forensic anthropology. Int J Legal Med 2017;131(6):1675–90. http://dx.doi.org/10.1007/s00414-017-1555-0.
[76] Bertsatos A, Chovalopoulou M-E, Brůžek J. Advanced procedures for skull sex estimation using sexually dimorphic morphometric features. Int J Legal Med 2020;134(5):1927–37. http://dx.doi.org/10.1007/s00414-020-02334-9.
[77] Uteuliyeva M, Zhumekenov A, Takhanov R, Assylbekov Z, Castro AJ, Kabdolov O. Fourier neural networks: A comparative study. Intell Data Anal 2020;24(5):1107–20. http://dx.doi.org/10.3233/IDA-195050.
[78] Optuna Development Team. Optuna: A hyperparameter optimization framework. 2023, [accessed 25 July 2025], https://optuna.org/.
[79] Forsyth DA, Mundy JL, di Gesú V, Cipolla R, LeCun Y, et al. Object recognition with gradient-based learning. Shape, Contour Group Comput Vis 1999;319–45. http://dx.doi.org/10.1007/3-540-46805-6.
[80] Kingma DP, Ba J. Adam: A method for stochastic optimization. 2017, http://dx.doi.org/10.48550/arXiv.1412.6980, arXiv preprint arXiv:1412.6980.
[81] Bergholm V, Izaac J, Schuld M, Gogolin C, Ahmed S, et al. Pennylane: Automatic differentiation of hybrid quantum-classical computations. 2018, http://dx.doi.org/10.48550/arXiv.1811.04968, arXiv preprint arXiv:1811.04968.
[82] IBM. IBM quantum. 2021, [Accessed 26 July 2025]. https://quantum.ibm.com/.
[83] Javadi-Abhari A, Treinish M, Krsulich K, Wood CJ, Lishman J, et al. Quantum computing with Qiskit. 2024, http://dx.doi.org/10.48550/arXiv.2405.08810, arXiv preprint arXiv:2405.08810.
[84] Lefèvre T, Tournois L. Artificial Intelligence and Diagnostics in Medicine and Forensic Science. Diagnostics 2023;13(23):3554. http://dx.doi.org/10.3390/diagnostics13233554.
[85] Thurzo A, Kosnáčová HS, Kurilová V, Kosmel' S, Beňuš R, et al. Use of advanced artificial intelligence in forensic medicine, forensic anthropology and clinical anatomy. Healthcare 2021;9(11):1545. http://dx.doi.org/10.3390/healthcare9111545.
[86] Zhou Y, Zhang J, Huang J, Deng K, Zhang J, et al. Digital whole-slide image analysis for automated diatom test in forensic cases of drowning using a convolutional neural network algorithm. Forensic Sci Int 2019;302:109922. http://dx.doi.org/10.1016/j.forsciint.2019.109922.
[87] Zeng Y, Zhang X, Yoshizumi I, Zhang Z, Mizuno T, et al. Deep learning-based diagnosis of fatal hypothermia using post-mortem computed tomography. Tohoku J Exp Med 2023;260(3):253–61. http://dx.doi.org/10.1620/tjem.2023.J041.
[88] Falissard L, Morgand C, Roussel S, Imbaud C, Ghosn W, et al. A deep artificial neural network- based model for prediction of underlying cause of death from death certificates: algorithm development and validation. JMIR Med Informatics 2020;8(4):e17125. http://dx.doi.org/10.2196/17125.
[89] Byeon W, Dominguez-Rodrigo M, Arampatzis G, Baquedano E, Yravedra J, et al. Automated identification and deep classification of cut marks on bones and its paleoanthropological implications. J Comput Sci 2019;32:36–43. http://dx.doi.org/10.1016/j.jocs.2019.02.005.
[90] Savakar DG, Kannur A. Ensemble learning approach for weapon recognition using images of wound patterns: A forensic perspective. Int J Image, Graph Signal Process 2018;11(11):1. http://dx.doi.org/10.5815/ijigsp.2018.11.01.
[91] Panahi F, Rashidi S, Sheikhani A. Application of the Fractional Fourier Transform for Feature Extraction from Electrocardiogram and Galvanic Skin Response in Emotion Recognition. Biomed Signal Process Control 2021;69:102863. http://dx.doi.org/10.1016/j.bspc.2021.102863.
[92] Tancik M, Srinivasan P, Mildenhall B, Fridovich-Keil S, Raghavan N, et al. Fourier features let networks learn high frequency functions in low dimensional domains. Adv Neural Inf Process Syst 2020;33:7537–47. http://dx.doi.org/10.5555/3495724.3496356.
[93] Dağı GE, Gökçay E, Tora H. Fourier-Based Image Classification Using CNN. J Sci Technol Eng Res 2024;5(1):92–101. http://dx.doi.org/10.53525/jster.1501920.
[94] Canto AC, Kaur J, Kermani MM, Azarderakhsh R. Algorithmic security is insufficient: A comprehensive survey on implementation attacks haunting post-quantum security. 2023, http://dx.doi.org/10.48550/arXiv.2305.13544, arXiv preprint arXiv:2305.13544.
[95] Sanal P, Karagoz E, Seo H, Azarderakhsh R, Mozaffari-Kermani M. Kyber on ARM64: Compact implementations of Kyber on 64-bit ARM Cortex-A processors. In: International conference on security and privacy in communication systems. Springer; 2021, p. 424–40. http://dx.doi.org/10.1007/978-3-030-90022-9.
[96] Koziel B, Azarderakhsh R, Kermani MM. A high-performance and scalable hardware architecture for isogeny-based cryptography. IEEE Trans Comput 2018;67(11):1594–609. http://dx.doi.org/10.1109/TC.2018.2815605.
[97] Koziel B, Ackie A-B, El Khatib R, Azarderakhsh R, Kermani MM. SIKE'd up: Fast hardware architectures for supersingular isogeny key encapsulation. IEEE Trans Circuits Syst I Regul Pap 2020;67(12):4842–54. http://dx.doi.org/10.1109/TCSI.2020.2992747.
[98] Jalali A, Azarderakhsh R, Kermani MM, Jao D. Supersingular isogeny diffie-hellman key exchange on 64-bit ARM. IEEE Trans Dependable Secur Comput 2017;16(5):902–12. http://dx.doi.org/10.1109/TDSC.2017.2723891.
[99] Azarderakhsh R, Järvinen KU, Mozaffari-Kermani M. Efficient algorithm and architecture for elliptic curve cryptography for extremely constrained secure applications. IEEE Trans Circuits Syst I Regul Pap 2014;61(4):1144–55. http://dx.doi.org/10.1109/TCSI.2013.2283691.
[100] Kermani MM, Reyhani-Masoleh A. Parity-based fault detection architecture of S-box for advanced encryption standard. In: 2006 21st IEEE international symposium on defect and fault tolerance in VLSI systems. IEEE; 2006, p. 572–80. http://dx.doi.org/10.1109/DFT.2006.50.
[101] Bayat-Sarmadi S, Mozaffari-Kermani M, Reyhani-Masoleh A. Efficient and concurrent reliable realization of the secure cryptographic SHA-3 algorithm. IEEE Trans Comput-Aided Des Integr Circuits Syst 2014;33(7):1105–9. http://dx.doi.org/10.1109/TCAD.2014.2307002.
[102] Cintas-Canto A, Mozaffari-Kermani M, Azarderakhsh R. Reliable code-based post-quantum cryptographic algorithms through fault detection on FPGA. In: 2023 IEEE nordic circuits and systems conference (norCAS). IEEE; 2023, p. 1–5. http://dx.doi.org/10.1109/NorCAS58970.2023.
[103] Cintas-Canto A, Kermani MM, Azarderakhsh R. Error detection constructions for ITA finite field inversions over GF(2^m) on FPGA using CRC and Hamming codes. IEEE Trans Reliab 2022;72(2):651–61. http://dx.doi.org/10.1109/TR.2022.3216014.
[104] Coecke B, Duncan R. Interacting quantum observables. In: International colloquium on automata, languages, and programming. Springer; 2008, p. 298–310. http://dx.doi.org/10.1007/978-3-540-70583-3_25.
[105] van de Wetering J. ZX-calculus for the working quantum computer scientist. 2020, http://dx.doi.org/10.48550/arXiv.2012.13966, arXiv preprint arXiv:2012.13966.
[106] Amari S-I. Natural gradient works efficiently in learning. Neural Comput 1998;10(2):251–76. http://dx.doi.org/10.1162/089976698300017746.
[107] Abbas A, Sutter D, Zoufal C, Lucchi A, Figalli A, et al. The power of quantum neural networks. Nat Comput Sci 2021;1(6):403–9. http://dx.doi.org/10.1038/s43588-021-00056-2.
[108] McClean JR, Boixo S, Smelyanskiy VN, Babbush R, Neven H. Barren plateaus in quantum neural network training landscapes. Nat Commun 2018;9(1):4812. http://dx.doi.org/10.1038/s41467-018-07090-4.
[109] Schuld M, Sweke R, Meyer JJ. Effect of data encoding on the expressive power of variational quantum-machine-learning models. Phys Rev A 2021;103(3):032430. http://dx.doi.org/10.1103/PhysRevA.103.032430.
[110] Demšar J. Statistical comparisons of classifiers over multiple data sets. J Mach Learn Res 2006;7(Jan):1–30. http://dx.doi.org/10.5555/1248547.1248548.
[111] Rainio O, Teuho J, Klén R. Evaluation metrics and statistical tests for machine learning. Sci Rep 2024;14(1):6086. http://dx.doi.org/10.1038/s41598-024-56706-x.
[112] Cohen J. Statistical power analysis for the behavioral sciences. Routledge; 2013, http://dx.doi.org/10.4324/9780203771587.